ELSEVIER

Contents lists available at ScienceDirect

Journal of Alloys and Compounds

journal homepage: http://www.elsevier.com/locate/jalcom



Microstructure and martensitic transformation of NiTiHfSc high temperature shape memory alloys



X.M. Fan a, S.Y. Sun a, Y.X. Tong a, *, L. Li a, B. Tian a, F. Chen a, Y.F. Zheng b

- ^a Institute of Materials Processing and Intelligent Manufacturing, College of Materials Science and Chemical Engineering, Harbin Engineering University, Harbin. 150001. China
- ^b Department of Materials Science and Engineering, College of Engineering, Peking University, Beijing, 100871, China

ARTICLE INFO

Article history:
Received 27 June 2018
Received in revised form
19 November 2018
Accepted 21 November 2018
Available online 22 November 2018

Keywords:
Intermetallics
NiTiHfSc high temperature shape memory alloys
Phase transitions
Microstructure

ABSTRACT

In present work, microstructure and martensitic transformation of $Ni_{49}Ti_{36-x}Hf_{15}Sc_x(x=0,0.5,1,2$ at.%) alloys were investigated. The results show that the Sc addition significantly influences the microstructure of the alloy. After the addition of Sc, Sc_2O_3 phase presents besides B19' martensite and $(Ti,Hf)_2Ni$ phase at room temperature. When the Sc content is no less than 1 at.%, the chain-like morphology of $(Ti,Hf)_2Ni$ phase changes to spherical-like one. Upon cooling and heating, these alloys show single-step martensitic transformation and its reverse transformation. With increasing Sc content, the transformation temperatures are reduced at a rate of 21 °C per 1 at.%Sc resulting from the reduced (Ti+Hf+Sc)/Ni ratio. The addition of Sc is effective in improving the thermal cycling stability of martensitic transformation because of the solid-solution strengthening of Sc. After ten cycles, the change of transformation peak temperature of $Ni_{49}Ti_{35.5}Hf_{15}Sc_{0.5}$ alloy is only 4.7 °C.

© 2018 Elsevier B.V. All rights reserved.

1. Introduction

In past decades, high temperature shape memory alloys (HTSMAs) have received much attention from various engineering fields, such as aerospace, automobile, oil and gas industries, because of their shape memory effect and superelasticity at temperatures above $100\,^{\circ}\text{C}$ [1–3]. Among the reported HTSMAs, NiTiHf alloys have been regarded as the most promising candidates for practical applications working in the range of $100-300\,^{\circ}\text{C}$ due to their controllable martensitic transformation temperature, considerable shape recovery properties, high work output and lower cost compared with TiNiX(X = Pt, Pd, Au) alloys [4–6]. Generally speaking, most of the superior properties of shape memory alloys (SMAs) are related to the thermoelastic martensitic transformation which can be effectively tailored by alloying.

Until now, several fourth elements have been added into NiTiHf alloys, including Cu [7,8], Pd [9], Nb [10], Ta [11], Y [12], Ag and Sn [13] as well as Zr [14]. The additions of the above-mentioned elements, with the exception of Zr, reduce transformation

E-mail address: tongyx@hrbeu.edu.cn (Y.X. Tong).

temperature to different extents [7–13]. For example, after the addition of 15 at.% Nb, the martensitic transformation start temperature (M_s) of Ni_{49.5}Ti_{35.5}Hf₁₅ alloy decreases from 189 °C to 72 °C under an applied stress of 100 MPa [10]. As compared with other elements, the Zr addition takes a different role which elevates the transformation temperature of NiTiHf alloys. With increasing Zr content from 0 to 15 at.%, the reverse transformation start temperature (A_s) of Ni₅₀Ti_{38-x}Hf₁₂Zr_x obviously increases from 107 °C to 557 °C [14]. In addition, the proper additions of Cu, Sn and Zr may cause multiple-step martensitic transformation and its reverse transformation [8,13,14].

Sc is also one of the important alloying elements of NiTi-based SMAs. First principle calculation shows that Sc tends to occupy Ti site rather than Ni site in NiTi lattice since the formation energy of substituting of Sc for Ti is less than that of substituting of Sc for Ni [15,16]. With respect to experimental results, the effect of Sc addition on martensitic transformation of NiTi-based alloys remains disputed to date. Kudryavtsev et al. reported that $M_{\rm S}$ of equiatomic NiTi alloy is reduced by the addition of Sc (20 °C per 1 at% Sc) [17]. Xi et al. reported an opposite dependence of Sc addition on $M_{\rm S}$ [16]. Atli et al. found that Ti₅₀Ni_{24.5}Pd₂₅Sc_{0.5} alloy shows slightly lower transformation temperatures, nearly equal transformation hysteresis and enhanced shape recovery properties in comparison with Ti_{50.5}Ni_{24.5}Pd₂₅ alloy [18]. Thus, it is expected

^{*} Corresponding author. Institute of Materials Processing and Intelligent Manufacturing, College of Materials Science and Chemical Engineering, Harbin Engineering University, No.145 Nantong Street, Harbin, 150001, China.

that the Sc addition may significantly influence martensitic transformation of NiTiHf HTSMAs. One of the drawbacks of NiTiHf alloys is the poor cycling stability of martensitic transformation [4,19]. This may be modified by the Sc addition because of solid-solution strengthening effect. However, as yet, no reports on microstructure and martensitic transformation of NiTiHfSc alloys are available.

In the present work, Ni-lean Ni $_{49}$ Ti $_{36}$ Hf $_{15}$ alloy was chosen as the starting material because it shows the desirable transformation temperatures in the range of $100-300\,^{\circ}$ C. Sc was added into this alloy at the expense of Ti. The effect of Sc addition on microstructure and martensitic transformation of NiTiHfSc alloys was systematically investigated. The particular attention was place on the effect of Sc content on phase transformation and its thermal cycling stability.

2. Experimental

A series of NiTiHfSc alloys with nominal compositions of Ni $_{49}$ Ti $_{36-x}$ Hf $_{15}$ Sc $_x$ (x = 0, 0.5, 1, 2 at.%) ingots were arc-melted by using high purity raw materials. For simplicity, these alloys for x = 0, 0.5, 1, 2 at.% were represented by Hf15Sc0, Hf15Sc0.5, Hf15Sc1 and Hf15Sc2 hereafter. In order to achieve compositional homogeneity, the ingots were re-melted six times. A pure Ti button used as an oxygen-getter was also melted before the melting of NiTiHfSc alloys. After melting, the ingots were solution-treated at 960 °C for 3 h in vacuum and then quenched into water.

Phase transformation behavior was investigated by differential scanning calorimetry (DSC) using a Perkin Elmer diamond instrument with heating and cooling rates of 20 °C/min. The sample mass is between 20 and 30 mg. Microstructural and chemical analyses were carried out on a JEOL JXA-8230 electron probe micro-analyzer (EPMA) equipped with wave-length dispersive X-ray spectrometers (WDS). The operating voltage is 15 kV. Transmission electron microscopy (TEM) observations were conducted using a JEOL 2100 microscope (TEM) which was operated at 200 kV with a double-tilt sample stage. The foils for TEM observation were prepared by mechanical grinding and twin-jet electropolishing. The electrolyte solution consists of 95% acetic acid and 5% perchloric acid in volume. X-ray diffraction (XRD) was carried out on a PANalytical Xpert'pro diffractometer using Cu Kα radiation by step-scanning in the 20 range of 20-80°. Vickers microhardness measurements were carried out with a loading of 200 g and a holding duration for 20 s at room temperature. At least ten points were measured and the average value was taken as the microhardness.

3. Results and discussion

Fig. 1 shows the XRD patterns of different NiTiHfSc alloys measured at room temperature. The pattern of Hf15Sc0 sample can be indexed as a mixture of B19' martensite and (Ti.Hf)₂Ni using the following lattice parameters: B19', a = 0.30108 nm $b = 0.40787 \,\mathrm{nm}$, $c = 0.48104 \,\mathrm{nm}$ and $\beta = 101.69^{\circ}$ and $(Ti, Hf)_2 Ni$, a = 1.1343 nm. The lattice parameters of B19' martensite are close to those previous reported by Potapov et al. [20] and Mehrdad Zarinejad et al. [21] and slightly different from that reported by Meng et al. [7,12] because of the slight difference in matrix composition. After the Sc addition, these alloys still mainly consist of B19' martensite and (Ti,Hf)₂Ni phase at room temperature and no additional phase can be identified from XRD patterns. This indicates that M_s of all samples is above room temperature. For NiTiHfSc alloys with different Sc contents, the detailed lattice parameters of B19' martensite of are listed in Table 1. In general, the Sc addition slightly increases the lattice parameters of B19' martensite. This is possible due to the larger atomic radius of Sc (0.16 nm) than those of Ti, Ni and Hf (0.14 nm, 0.135 nm and 0.155 nm).

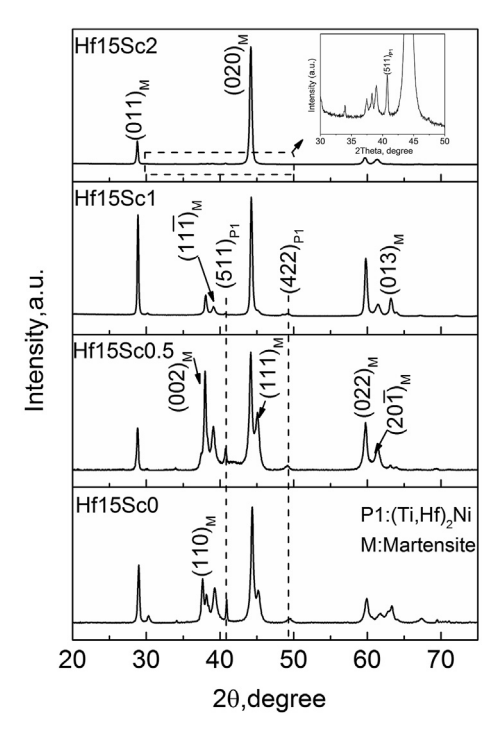


Fig. 1. XRD patterns of NiTiHfSc alloys with different Sc contents showing the phase constituent at room temperature. The inset is the enlargement of circled region.

Table 1Lattice parameters of B19' martensite for different NïTiHfSc alloys.

Alloy	a (nm)	b (nm)	c (nm)	β (°)
Hf15Sc0	0.30108	0.40787	0.48104	101.69
Hf15Sc0.5	0.30236	0.40971	0.48381	102.00
Hf15Sc1	0.30342	0.40939	0.48299	101.71
Hf15Sc2	0.30229	0.41199	0.48168	102.55

Fig. 2 shows the back-scattered electron (BSE) images of different NiTiHfSc samples. Microstructure of Hf15Sc0 sample is characterized by the black phase (P1) with irregular shape embedded into the B19' martensite matrix (M), as shown in Fig. 2(a). The P1 phase indicated by single arrow has a composition of 53.38 at.%Ti, 9.58 at.%Hf and 33.43 at.% Ni, hence can be regarded as (Ti,Hf)₂Ni phase, being consistent with the XRD results shown in Fig. 1 and the reported results [12]. Some of chain-like (Ti,Hf)₂Ni particles preferentially distribute along the grain boundaries [12], some of isolated particles distribute into the grains. After the Sc addition, small amount of Sc also dissolved into (Ti,Hf)₂Ni particles. Fig. 2(b)-(d) show that besides (Ti,Hf)₂Ni phase, some black particles (P2) present when the Sc was added. These particles were indicated by double-headed arrows. The P2 phase in Hf15Sc0.5 sample mainly consists of Sc and O with a composition of 60.12 at.% O, 34.91 at.% Sc, 0.87 at.% Hf, 1.94 at.% Ti and 2.15 at.% Ni and is regarded as Sc₂O₃ phase. The formation of Sc₂O₃ phase in TiNiPdSc alloys has been reported and attributed to the strong affinity of Sc for residual oxygen [18,22]. The volume fraction of Sc₂O₃ phase is quite small, so that it was not detected by XRD measurement. When the Sc content is no less than 1 at.%, most of (Ti,Hf)2Ni phase changes from chain-like morphology to spherical shape. This is different from the effect of other alloying elements on microstructure of Ni₄₉Ti₃₆Hf₁₅ alloy, such as Cu [7], Y [12]. Some of Sc₂O₃ particles embedded into (Ti,Hf)₂Ni particles, as confirmed by the line scanning of consistent elements shown in Fig. 2(e) which is an enlargement of circled region in Fig. 2(d). This suggests that Sc₂O₃

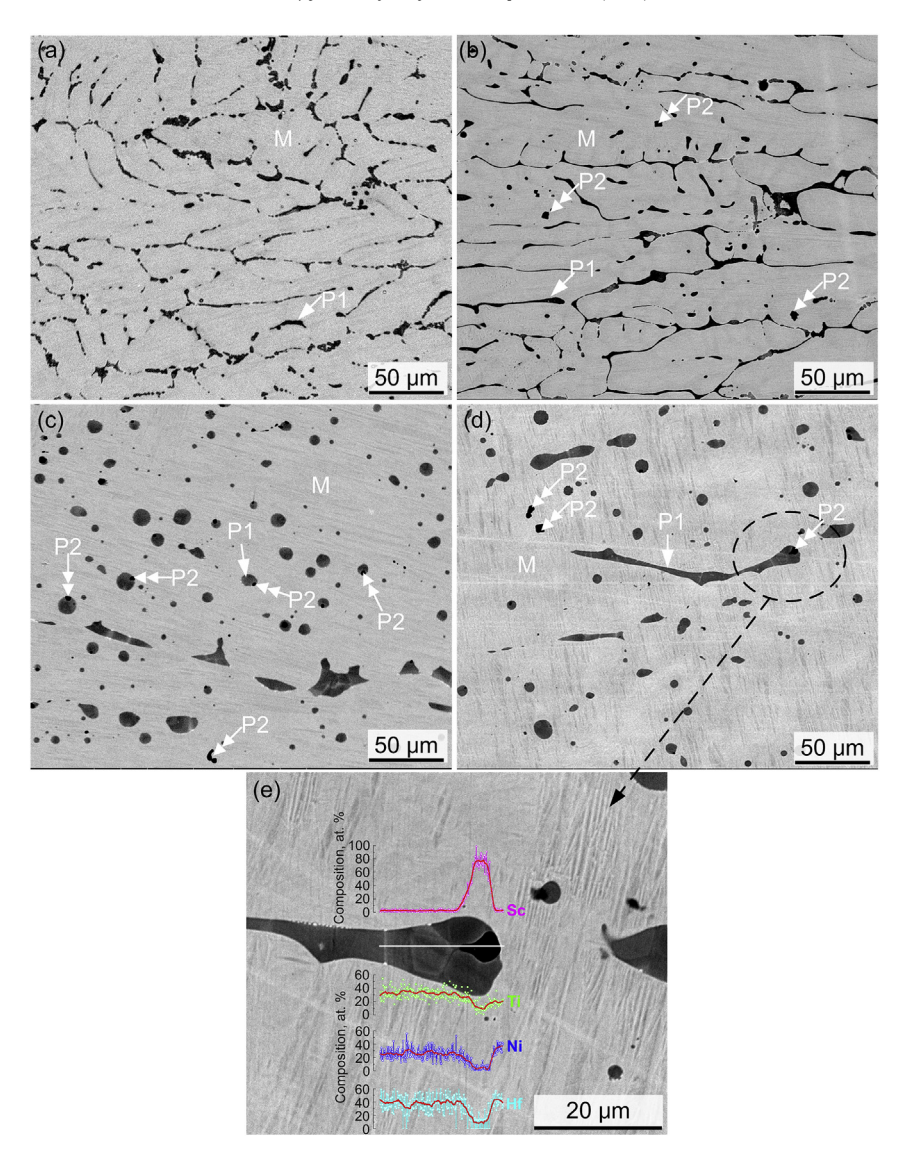


Fig. 2. BSE images of NiTiHfSc alloys with different Sc contents, (a) Hf15Sc0, (b) Hf15Sc0.5, (c) Hf15Sc1 and (d) Hf15Sc2. M, P1 and P2 stand for matrix, $(Ti,Hf)_2Ni$ phase and Sc_2O_3 phase, respectively.

phase may form prior to $(Ti,Hf)_2Ni$ phase during solidification. The above suggestion is supported by the fact that the formation energy of Sc_2O_3 phase is much lower than that of Ti_2Ni phase [23]. Some of $(Ti,Hf)_2Ni$ particles preferentially nucleate at the interface between Sc_2O_3 and matrix once Sc_2O_3 phase presents during solidification. This may change the morphology and distribution of $(Ti,Hf)_2Ni$ phase and implies that the Sc addition can be used to tailor the microstructure of NiTiHf-based HTSMAs, thus control the mechanical properties. The chemical composition of different phases determined through WDS is summarized in Table 2.

Microstructure of NiTiHfSc alloy was further investigated by TEM observation. Fig. 3 shows the representative bright field images of Hf15Sc0 and Hf15Sc2 samples. The selected area electron diffraction (SAED) patterns are also presented. The Sc addition does not obviously change the morphology of martensite. The martensitic variants characterized by the lath-like morphology are well accommodated. The variant boundary is well-defined, indicating the good mobility. The SAED pattern in Fig. 3(c) shows that the martensite substructure is mainly (001) compound twin. The variants are related to the (011) type I twin, which is confirmed by the pattern shown in Fig. 3(d) which was taken from the interface

Table 2Compositional analysis results of different phases for NiTiHfSc alloys with different Sc contents. The composition is in at.%.

Phase	Alloy	Ti	Ni	Hf	Sc	0	(Ti+Hf+Sc)/Ni
Matrix	Hf15Sc0	37.42	49.21	13.37	_	_	1.032
	Hf15Sc0.5	36.95	49.35	13.26	0.44	_	1.026
	Hf15Sc1	36.04	49.42	13.49	1.03	_	1.023
	Hf15Sc2	35.00	49.46	13.49	2.05	_	1.022
P1	Hf15Sc0	53.38	33.43	9.58	_	_	_
	Hf15Sc0.5	55.48	34.78	9.54	0.20	_	_
	Hf15Sc1	56.86	32.59	10.13	0.43	_	_
	Hf15Sc2	56.64	32.54	9.93	0.90	_	_
P2	Hf15Sc0	_	_	_	_	_	_
	Hf15Sc0.5	1.94	2.15	0.87	34.91	60.12	_
	Hf15Sc1	0.12	0.40	0.27	37.50	61.71	_
	Hf15Sc2	0.51	0.40	0.39	35.82	62.12	_

of variants. The above results are consistent with the previous findings of NiTiHf-based alloys [12,24,25].

DSC curves of different samples are shown in Fig. 4. All of the samples show single-step $B2 \leftrightarrow B19'$ forward transformation and its

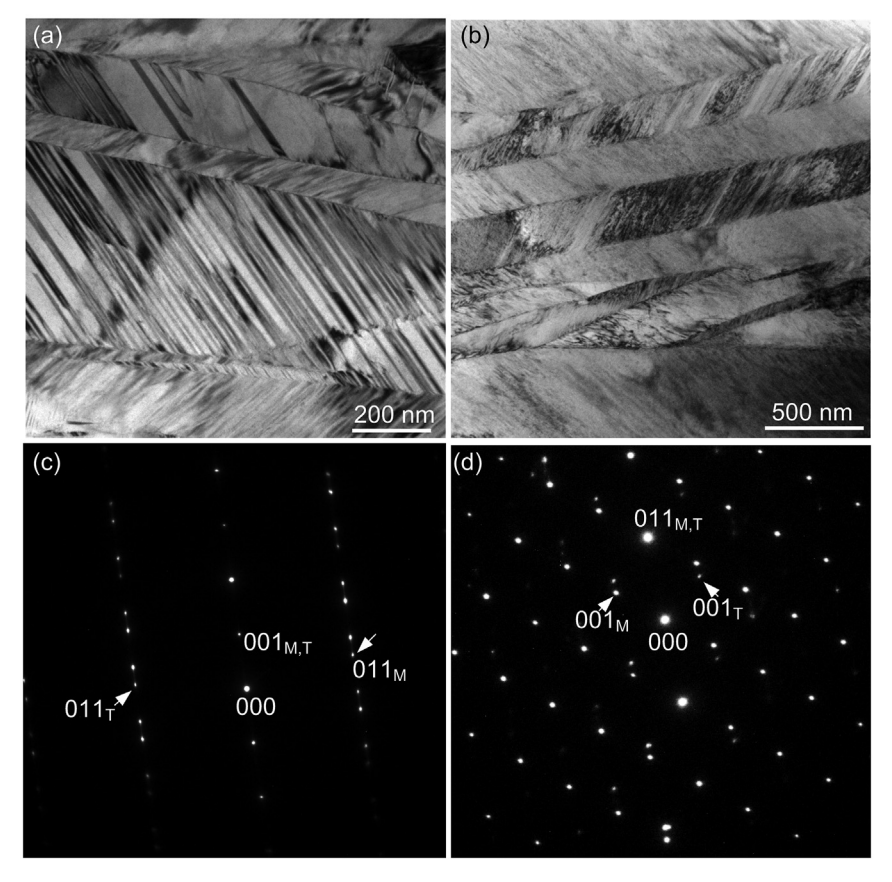


Fig. 3. TEM bright field images of Hf15Sc0 (a) and Hf15Sc2 (b) alloys and the SAED patterns taken from the interior of variant (c) and the variant interface (d) of (b).

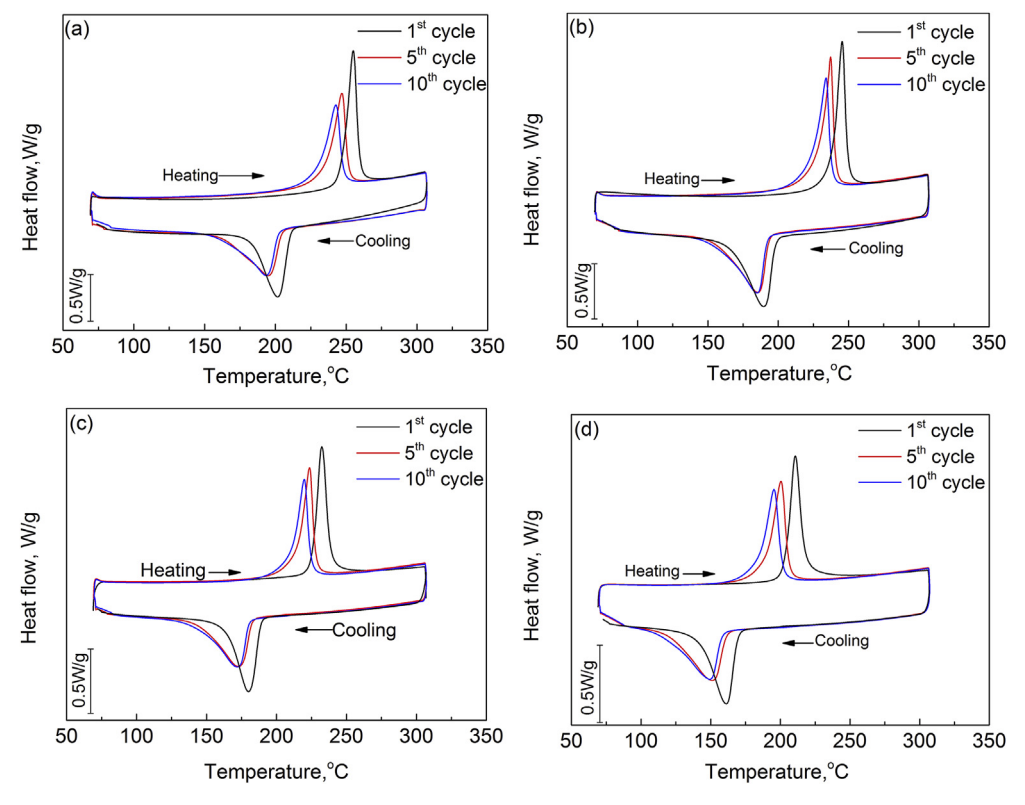


Fig. 4. DSC curves of NiTiHfSc alloys with different Sc contents, (a) Hf15Sc0, (b) Hf15Sc0.5, (c) Hf15Sc1 and (d) Hf15Sc2.

reverse transformation upon cooling and heating. The transformation peaks shift to low temperature side with increasing cycling number. It is generally accepted that R-phase transformation can be induced by thermal cycling in near-equiatomic NiTi alloy [26] and alloying, for example, the addition of Cu or Sn in Ni₄₀Ti₃₆Hf₁₅ alloy [8,13]. However, no R-phase transformation can be identified in the present samples. The dependence of Sc content on the characteristic temperatures of phase transformation for the first cycle is illustrated by Fig. 5, in which M_p is peak temperature of forward transformation, M_f is finish temperature of forward transformation, A_p is peak temperature of reverse transformation and A_f is finish temperature of reverse transformation. With increasing Sc content, the characteristic temperatures are monotonously reduced at a rate of about 21 °C per 1 at. %Sc. This rate agrees well with the previous results reported on NiTiSc alloys reported by Kudryavtsev et al. [17] and Ti₅₀Ni_{24.5}Pd₂₅Sc_{0.5} alloy [18], but is lower than that in case of Ti_{49.3}Ni_{24.7}Pd_{25.0}Sc_{1.0} alloy in which $M_{\rm S}$ temperature was reduced at a rate of about 32 °C per 1 at.%Sc [22]. The Sc addition does not significantly influence the transformation hysteresis which is defined as the difference between A_p and M_p (A_p - M_p). The effect of Sc content on transformation temperature can be well explained by the change of matrix composition. In the present work, both Hf and Sc occupy Ti site in NiTi lattice [15]. According to the results in Table 2, the increase of Sc content results in the decrease of (Ti+Hf+Sc)/Ni ratio. Considering the fact that the transformation temperature of NiTi-based SMAs increases with increasing Ti/Ni ratio [1], it is concluded that the effect of Sc content on transformation temperature can be attributed to the change of matrix composition.

In order to evaluate the influence of Sc content on thermal cycling stability, the difference (ΔM_p) between M_p of the first cycle and the tenth cycle $(M_p^{1st}-M_p^{10th})$ was plotted as a function of Sc content, as shown in Fig. 6. The value of ΔM_p first decreases and then increases with increasing Sc content. The value of Hf15Sc0 sample is close to the reported results [12,24]. The Hf15Sc0.5 sample shows the minimum ΔM_p of 4.7 °C, implying that the proper addition of Sc is beneficial to enhancing the thermal cycling stability of martensitic transformation. This is similar to the effect of Cu addition [8] and opposite to that of Y addition [12].

The thermal cycling stability is generally related to the introduction of dislocations, which usually compensate the incompatibility between martensite and parent phase during transformation [27,28]. In order to suppress the generation and movement of dislocations, various physical metallurgy methods

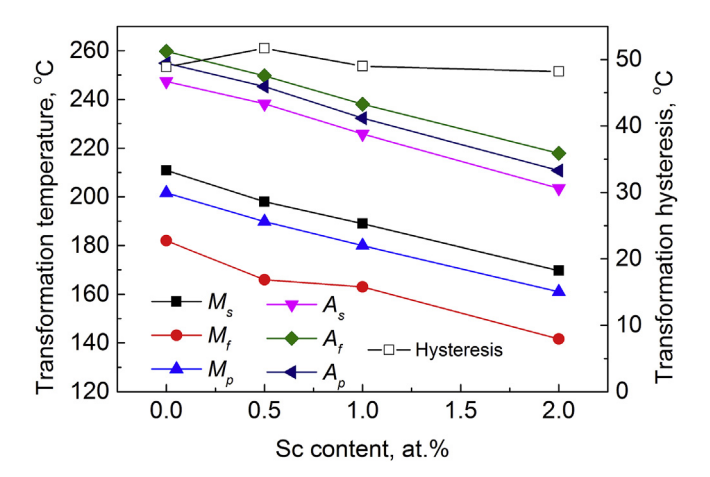


Fig. 5. Effect of Sc content on transformation temperatures and transformation hysteresis of different NiTiHfSc alloys. The transformation temperatures were determined from the DSC curves of first cycle.

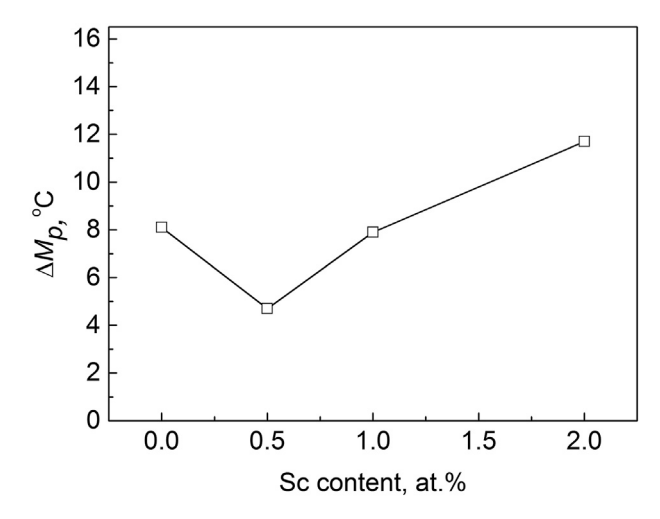


Fig. 6. Effect of Sc content on $\Delta M_{\rm p}$ of NiTiHfSc alloys with different Sc contents.

have been used to strengthen the matrix, including grain refinement [26,28,29], aging of Ni-rich TiNi-based alloys and coldworking [27] etc. For Ni-lean NiTiHf alloys, equal channel angular pressing, one of several plastic deformation methods, has been successfully used to refine the microstructure and enhance the thermal cycling stability [29]. For Ni-rich NiTiHf alloys, aging strengthening through H-precipitate is also effective in improving the cycling stability [30]. In the present work, grain refinement and aging strengthening are not applicable since the samples are solution-treated at the same condition. Therefore, other strengthening mechanism is possibly related to the results shown in Fig. 6. It has been reported that the Sc addition may increase the mechanical strength by solid-solution strengthening for Ti_{50.5}Ni_{24.5}Pd₂₅ alloy [18]. The same mechanism is also suggested to be effective for NiTiHf alloys. In order to confirm this hypothesis, microhardness measurements were carried out at room temperature. The results are shown in Fig. 7 as a function of Sc content. The microhardness was observed to first increase and then decrease with increasing Sc content. The Hf15Sc0.5 sample shows the largest microhardness. This means that the proper addition of Sc enhances the strength of NiTiHfSc alloy. It is noted that the effect of Sc content on microhardness shows an opposite tendency compared with that of ΔM_p

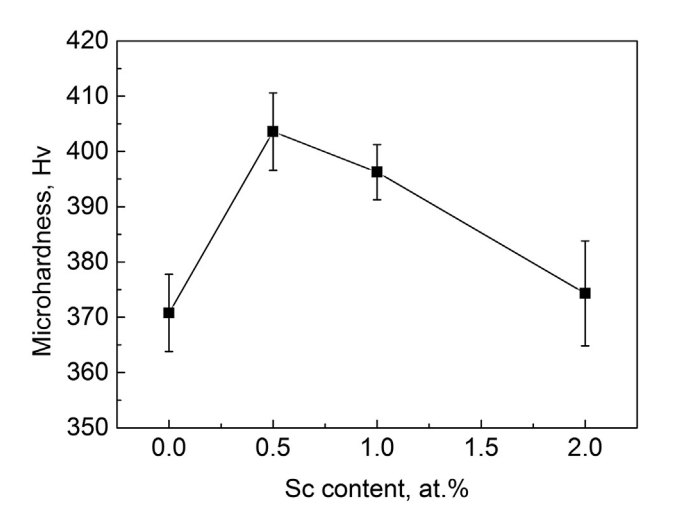


Fig. 7. Effect of Sc content on microhardness of NiTiHfSc alloys with different Sc contents.

(Fig. 6). This may imply that the solid-solution strengthening resulting from Sc addition is responsible for the enhanced thermal cycling stability of martensitic transformation.

The dependence of microhardness on Sc content can be rationalized by considering the effects of solid-solution strengthening and microstructural change resulting from Sc addition. In NiTiHf alloys, the chain-like (Ti,Hf)₂Ni phase usually distributes along grain boundaries [12]. After addition of 0.5 at.% Sc. most of (Ti,Hf)₂Ni phase is still characterized by chain-like morphology. As compared to Hf15Sc0 alloy, the grain size of Hf15Sc0.5 alloy does not change too much. The microhardness increases due to the solid-solution strengthening of Sc. With further increase of Sc content, the morphology and distribution of (Ti,Hf)2Ni phase change, as shown in Fig. 2. This may suggest that the grain size of Hf15Sc1 and Hf15Sc2 samples is larger than that of Hf15Sc0 because of the absence of pinning from chain-like (Ti,Hf)₂Ni phase which usually distributes along grain boundaries. Furthermore, the distance between different particles increased with increasing Sc content from 1 to 2 at.%. Therefore, it is suggested that both the above two microstructural factors lead to the decrease of microhardness, which imposes an overwhelming effect on microhardness as compared with solid-solution strengthening of Sc.

Fig. 8 compares the thermal cycling stability of martensitic transformation of Hf15Sc0.5 sample with the reported results on Ni-lean NiTiHf-based HTSMAs, as demonstrated by ΔM_p . It should be pointed out that only three cooling and heating cycles were conducted on Ni_{49.8}Ti_{42.2}Hf₈ alloy [29]. For other reported alloys, the thermal cycling number is ten. The line segments between M_n of the first cycle and the tenth cycle (third for Ni_{49.8}Ti_{42.2}Hf₈ alloy) for different alloys were plotted to visually show ΔM_p . The value of ΔM_p are also shown. Interestingly, ΔM_p of Hf15Sc0.5 alloy is much smaller than those of reported values, indicating that martensitic transformation of this alloy has the best thermal cycling stability among the reported results. To the best of our knowledge, martensitic transformation of Ni₄₀Cu₁₀Ti₄₀Hf₁₀ alloy shows the best thermal cycling stability among the previous results reported in Nilean NiTiHf-based SMAs, which is evidenced by the small ΔM_n of about 5.2 °C [31]. However, the transformation temperatures of Ni₄₀Cu₁₀Ti₄₀Hf₁₀ alloy are far below 100 °C [31]. Therefore, its data was not included into Fig. 8. As compared to Ni₄₀Cu₁₀Ti₄₀Hf₁₀ alloy, the present Hf15Sc0.5 alloy has a combination of higher transformation temperatures and better thermal cycling stability, which is beneficial to the design of actuators based on HTSMAs.

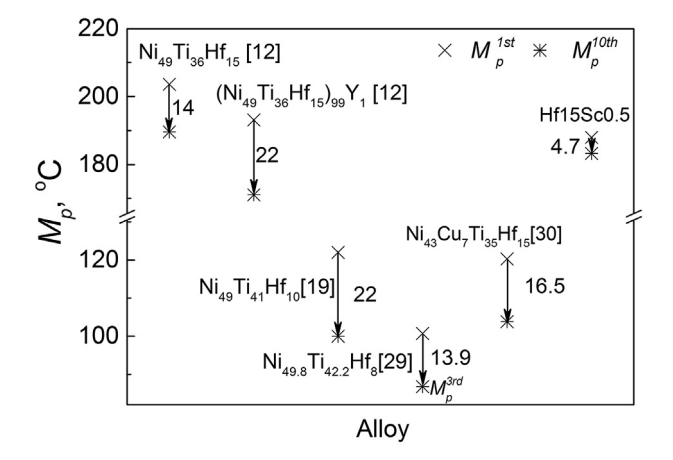


Fig. 8. Comparison of thermal cycling stability of martensitic transformation of Hf15Sc0.5 sample with the previously reported results on Ni-lean NiTiHf alloys. This was demonstrated by the marked ΔM_p .

4. Conclusions

The effect of Sc addition on microstructure and martensitic transformation of $Ni_{49}Ti_{36-x}Hf_{15}Sc_x(x=0,\ 0.5,\ 1,\ 2\ at.\%)$ alloys has been systematically investigated and the results are summarized as follows:

- (1) Microstructure of Ni₄₉Ti₃₆Hf₁₅ alloy consists of B19′ martensite matrix and (Ti,Hf)₂Ni phase at room temperature. After adding Sc, the alloys contain B19′ martensite, (Ti,Hf)₂Ni phase and Sc₂O₃ phase. In the meantime, the chain-like (Ti,Hf)₂Ni phase changes to spherical-like one.
- (2) Martensite of $Ni_{49}Ti_{36-x}Hf_{15}Sc_x$ alloys shows the lath-like plates which are mainly characterized by (001) compound twin substructure and related to (011) type I twinning mode.
- (3) Martensitic transformation of $Ni_{49}Ti_{36-x}Hf_{15}Sc_x$ alloys is characterized by single-step transformation. With increasing Sc content, the transformation temperatures are reduced at a rate of about 21 °C/min per 1 at.%Sc due to the reduced (Ti+Hf+Sc)/Ni ratio.
- (4) The proper addition of Sc is beneficial to improving the thermal cycling stability of martensitic transformation for Ni₄₉Ti_{36-x}Hf₁₅Sc_x alloys. This can be attributed to the solidsolution strengthening of Sc.

Acknowledgements

This work was supported by National Natural Science Foundation of China [grant number 51671064], the Fundamental Research Funds for the Central Universities [grant number HEUCFP201730] and Key Laboratory of Superlight Materials & Surface Technology (Harbin Engineering University), Ministry of Education, China.

References

- K. Otsuka, X. Ren, Physical metallurgy of Ti-Ni-based shape memory alloys, Prog. Mater. Sci. 50 (2005) 511–678.
- [2] J. Ma, I. Karaman, R.D. Noebe, High temperature shape memory alloys, Int. Mater. Rev. 55 (2010) 257–315.
- [3] L. Casalena, G.S. Bigelow, Y. Gao, O. Benafan, R.D. Noebe, Y. Wang, M.J. Mills, Mechanical behavior and microstructural analysis of NiTi-40Au shape memory alloys exhibiting work output above 400 °C, Intermetallics 86 (2017) 33–44.
- [4] H.E. Karaca, E. Acar, H. Tobe, S.M. Saghaian, NiTiHf-based shape memory alloys, Mater. Sci. Technol. 30 (13) (2014) 1530–1544.
- [5] Y. Tong, F. Chen, B. Tian, L. Li, Y. Zheng, Microstructure and martensitic transformation of Ti₄₉Ni_{51-x}Hf_x high temperature shape memory alloys, Mater. Lett. 63 (2009) 1869–1871.
- [6] X.L. Meng, Y.F. Zheng, Z. Wang, L.C. Zhao, Shape memory properties of the $Ti_{36}Ni_{49}Hf_{15}$ high temperature shape memory alloy, Mater. Lett. 45 (2000) 128–132.
- [7] X.L. Meng, Y.X. Tong, K.T. Lau, W. Cai, L.M. Zhou, L.C. Zhao, Effect of Cu addition on phase transformation of Ti-Ni-Hf high-temperature shape memory alloys, Mater. Lett. 57 (2002) 452–456.
- [8] X.L. Meng, W. Cai, K.T. Lau, L.C. Zhao, L.M. Zhou, Phase transformation and microstructure of quaternary TiNiHfCu high temperature shape memory alloys, Intermetallics 13 (2005) 197–201.
- [9] H.E. Karaca, E. Acar, G.S. Ded, B. Basaran, H. Tobe, R.D. Noebe, G. Bigelow, Y.I. Chumlyakov, Shape memory behavior of high strength NiTiHfPd polycrystalline alloys, Acta Mater. 61 (2013) 5036–5049.
- [10] H.Y. Kim, T. Jinguu, T.-h. Nam, S. Miyazaki, Cold workability and shape memory properties of novel Ti–Ni–Hf–Nb high-temperature shape memory alloys, Scripta Mater. 65 (2011) 846–849.
- [11] R.V.S. Prasad, C.H. Park, S.-W. Kim, J.K. Hong, J.-T. Yeom, Microstructure and phase transformation behavior of a new high temperature NiTiHf-Ta shape memory alloy with excellent formability, J. Alloys Compd. 697 (2017) 55–61.
- [12] X. Yi, W. Gao, X. Meng, Z. Gao, W. Cai, L. Zhao, Martensitic transformation behaviors and mechanical properties of (Ti₃₆Ni₄₉Hf₁₅)_{100-x}Y_x high temperature shape memory alloys. I. Alloys Compd. 705 (2017) 98–104.
- ture shape memory alloys, J. Alloys Compd. 705 (2017) 98–104.

 [13] X. Yi, G. Pang, B. Sun, X. Meng, W. Cai, The microstructure and martensitic transformation behaviors in Ti-Ni-Hf-X (Ag, Sn) high temperature shape memory alloys, J. Alloys Compd. 756 (2018) 19–25.
- [14] S.H. Hong, J.T. Kim, H.J. Park, Y.S. Kim, J.Y. Suh, Y.S. Na, K.R. Lim, C.H. Shim, J.M. Park, K.B. Kim, Influence of Zr content on phase formation, transition and

- mechanical behavior of Ni-Ti-Hf-Zr high temperature shape memory alloys, I. Alloys Compd. 692 (2017) 77–85.
- [15] N. Singh, A. Talapatra, A. Junkaew, T. Duong, S. Gibbons, S. Li, H. Thawabi, E. Olivos, R. Arróyave, Effect of ternary additions to structural properties of NiTi alloys, Comput. Mater. Sci. 112 (2016) 347—355.
- [16] M. Xi, J. Shang, First principle study on NiTi alloyed with transition elements, Rare Metal Mater. Eng. 45 (8) (2016) 2041–2045.
- [17] Y.V. Kudryavtsev, E.L. Semenova, Effect of scandium and yttrium on martensitic transformations in tini-based alloys, Powder Metall. Met. Ceram. 48 (2009) 700–706.
- [18] K.C. Atli, I. Karaman, R.D. Noebe, A. Garg, Y.I. Chumlyakov, I.V. Kireeva, Improvement in the shape memory response of Ti_{50.5}Ni_{24.5}Pd₂₅ hightemperature shape memory alloy with Scandium microalloying, Metall. Mater. Trans. A 41 (10) (2010) 2485–2497.
- [19] S. Besseghini, E. Villa, Á. Tsuissi, Ni-Ti-Hf shape memory alloy: effect of aging and thermal cycling, Mater. Sci. Eng. A 273–275 (1999) 390–394.
- [20] P.L. Potapov, A.V. Shelyakov, A.A. Gulyaev, E.L. Svistunov, N.M. Matveeva, D. Hodgson, Effect of Hf on the structure of Ni-Ti martensitic alloys, Mater. Lett. 32 (1997) 247–250.
- [21] M. Zarinejad, Y. Liu, T.J. White, The crystal chemistry of martensite in NiTiHf shape memory alloys. Intermetallics 16 (7) (2008) 876–883.
- shape memory alloys, Intermetallics 16 (7) (2008) 876–883.

 [22] K.V. Ramaiah, C.N. Saikrishna, J. Bhagyaraj, Gouthama, S.K. Bhaumik, Influence of Sc addition on microstructure and transformation behaviour of Ni_{24,7}Ti_{50,3}Pd_{25,0} high temperature shape memory alloy, Intermetallics 40 (2013) 10–18.
- [23] I. Barin, Thermochemical Data of Pure Substances, VCH Verlagsgesellschaft, 1995 mbH.

- [24] H.E. Karaca, S.M. Saghaian, G. Ded, H. Tobe, B. Basaran, H.J. Maier, R.D. Noebe, Y.I. Chumlyakov, Effects of nanoprecipitation on the shape memory and material properties of an Ni-rich NiTiHf high temperature shape memory alloy, Acta Mater. 61 (2013) 7422—7431.
- [25] X.L. Meng, W. Cai, Y.D. Fu, J.X. Zhang, L.C. Zhao, Martensite structure in Ti-Ni-Hf-Cu quaternary alloy ribbons containing (Ti,Hf)₂Ni precipitates, Acta Mater. 58 (2010) 3751–3763.
- [26] Y.X. Tong, B. Guo, F. Chen, B. Tian, L. Li, Y.F. Zheng, E.A. Prokofiev, D.V. Gunderov, R.Z. Valiev, Thermal cycling stability of ultrafine-grained TiNi shape memory alloys processed by equal channel angular pressing, Scr. Mater. 67 (2012) 1–4.
- [27] S. Miyazaki, Y. Igo, K. Otsuka, Effect of thermal cycling on the transformation temperatures of Ti-Ni alloys, Acta Metall. 34 (1986) 2045–2051.
 [28] B. Kockar, I. Karaman, J.I. Kim, Y.I. Chumlyakov, J. Sharp, C.J. Yu, Thermo-
- [28] B. Kockar, I. Karaman, J.I. Kim, Y.I. Chumlyakov, J. Sharp, C.J. Yu, Thermomechanical cyclic response of an ultrafine-grained NiTi shape memory alloy, Acta Mater. 56 (14) (2008) 3630–3646.
- [29] B. Kockar, I. Karaman, J.I. Kim, Y. Chumlyakov, A method to enhance cyclic reversibility of NiTiHf high temperature shape memory alloys, Scr. Mater. 54 (12) (2006) 2203–2208.
 [30] H.E. Karaca, S.M. Saghaian, G. Ded, H. Tobe, B. Basaran, H.J. Maier, R.D. Noebe,
- [30] H.E. Karaca, S.M. Saghaian, G. Ded, H. Tobe, B. Basaran, H.J. Maier, R.D. Noebe, Y.I. Chumlyakov, Effects of nanoprecipitation on the shape memory and material properties of an Ni-rich NiTiHf high temperature shape memory alloy, Acta Mater. 61 (2013) 7422—7431.
- [31] X.L. Liang, Y. Chen, H.M. Shen, Z.F. Zhang, W. Li, Y.N. Wang, Thermal cycling stability and two-way shape memory effect of Ni-Cu-Ti-Hf alloys, Solid State Commun. 119 (2001) 381–385.